JOURNAL OF APPLIED CRYSTALLOGRAPHY

Volume 50 (2017)

Supporting information for article:

Concurrent Determination of Nanocrystal Shape and Amorphous Phases in Complex Materials by Diffraction Scattering Computed Tomography

Mie Elholm Birkbak, Ida Gjerlevsen Nielsen, Simon Frølich, Stuart R. Stock, Peter Kenesei, Jonathan D. Almer and Henrik Birkedal

Supporting information

S1. Details of Rietveld model

For the Rietveld refinements a pseudo-Voigt profile function in GSAS was used (Howard 1982, Thompson, Cox et al. 1987) to fit all phases. The following Rietveld Models were used:

Anatase: The structure from Rezaee *et al*. (Rezaee, Mousavi Khoie et al. 2011) was used with the unit cell parameters modified to $a = b = 3.780008$ Å and $c = 9.493167$ Å. An isotropic Lorentzian Scherrer broadening description of particle size was used (*LX*).

Rutile: The structure from Meagher *et al*. (Meagher and Lager 1979) was used with the unit cell parameters modified to $a = b = 4.587$ Å and $c = 2.953$ Å. An isotropic Lorentzian Scherrer broadening description of particle size was used (*LX*).

Maghemite: The structure from Jørgensen *et al*. (Jørgensen, Mosegaard et al. 2007) was used with the unit cell parameters modified to $a = b = c = 8.353327$ Å. An anisotropic Lorentzian Scherrer broadening description of particle size was used (*LX* and *PTEC* with the principal broadening axis [1 1 1]).

Hydroxyapatite: The structure from Veselinovic *et al*. (Veselinovic, Karanovic et al. 2010) was used with the unit cell parameters modified to $a = b = 9.415$ Å and $c = 6.869$ Å. An anisotropic Lorentzian Scherrer broadening description of particle size was used (*LX* and *PTEC* with the principal broadening axis [0 0 1]). Additionally, a parameter (*LY*) was used to describe microstrain broadening in HAP.

Representative plots of both voxels containing a mix of phases and one predominant constituent and the corresponding fit shows good descriptions of the data in all cases (Figure S1).

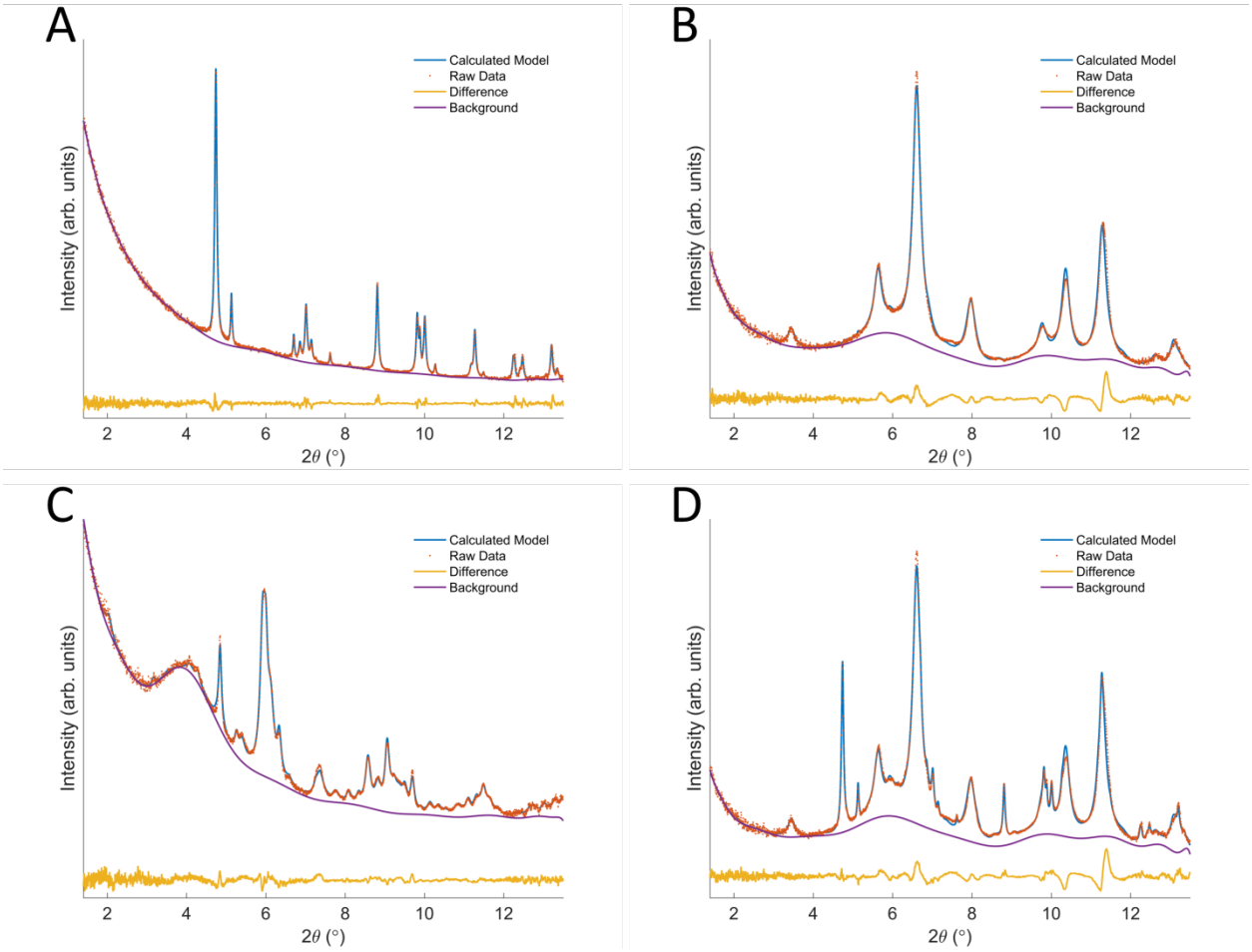

Figure S1 Representative plots of reconstructed data and the corresponding Rietveld model. The data is shown in red dots (·), the model in blue, the calculated difference in yellow and the background in purple. The background is further analysed using MCR-ALS. Voxel containing predominantly titania (A), maghemite (B), hydroxyapatite (C) and a mix of phases (D) are displayed.

S2. Peak overlap limiting nanoparticle peak broadening analysis

As noted in the main text, nanocrystal sizes for a given phase were almost the same throughout the sample, except in voxels containing phases with heavily overlapping peaks. Examples include the HAP-anatase and the rutile-maghemite mixtures. In the former case, the (021)/(002) peaks of HAP and the (101) peak of anatase overlap significantly; and this hinders fitting peak shapes in the affected voxels and leads to imprecise determination of nanocrystal sizes of HAP along [001]. In the second case, the heterogeneous size distribution originates from overlap of the (311) peak of maghemite and the (101) peak of rutile. The overlap complicates the determination of the rutile size, as the (101) is one of only two

strong peaks. The crystalline sizes of rutile, where no maghemite is present, also varied significantly compared to the other phases. However, the nanocrystal size of rutile is larger than the others, on the border of the experimental resolution, which means that a large variation in determined sizes can be expected.

S3. Crystalline phase weight fraction distributions and rutile to anatase ratios

Figure S2 shows the obtained weight fractions of the contributing phases. They are consistent with the known configuration of the sample and are less sensitive to the shadows and artifacts seen in the scale factor maps. Anatase and rutile from Degussa P25 were co-localized reflecting the intimate mixing of the two phases in the powder. The anatase/rutile ratio was approximately 80% and in voxels containing a low amount of titania only the anatase phase exceeded the criterion for further refinement resulting in seemingly missing rutile signals. We calculated a histogram of the anatase weight fraction in the TiO2 containing voxels. It is centered roughly around the expected 80% anatase with a mean value of 83.7%.

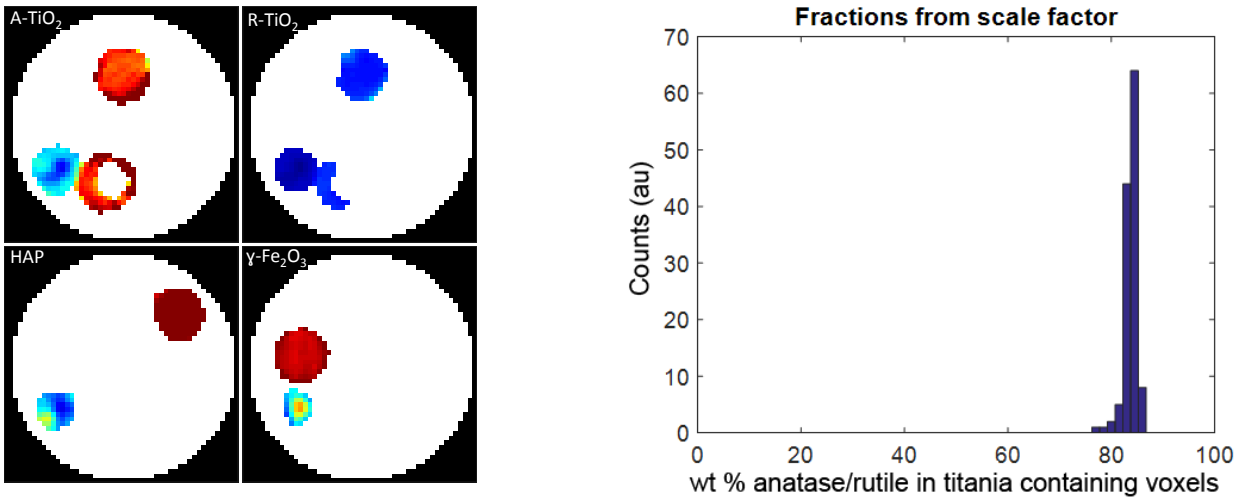

Figure S2 Weight fractions of crystalline phases determined by Rietveld refinement of DSCT data. The circular field of view is 1.4 mm in diameter. The right hand panel shows a histogram of the TiO_2 anatase wt%.

S4. MCR-ALS details

The MCR-ALS analysis was performed using the MCR-ALS GUI 2.0 software (Jaumot *et al.*, 2015). Four different components were assumed to contribute to the analyzed backgrounds from

the diffractograms. Including further components did not improve the description of the background. The scattering intensity of the components and their contribution to the total background signal was only restrained to be non-negative and normalized by the Euclidean mean. The scattering contribution of the four components were able to describe 99.9975% of the variance of the measured scattering intensity curve after crystalline peaks removal resulting in a relative error of residuals vs. experimental data of 0.6% resulting in a an excellent description of the data (Figure S3). The scattering of the four components contributing to the background was found to correspond to the expected scattering from glass, air, ACP and amorphous ferrihydrite, respectively. Furthermore, the spatial distribution of the phases is in precise correspondence with the sample design (see main text).

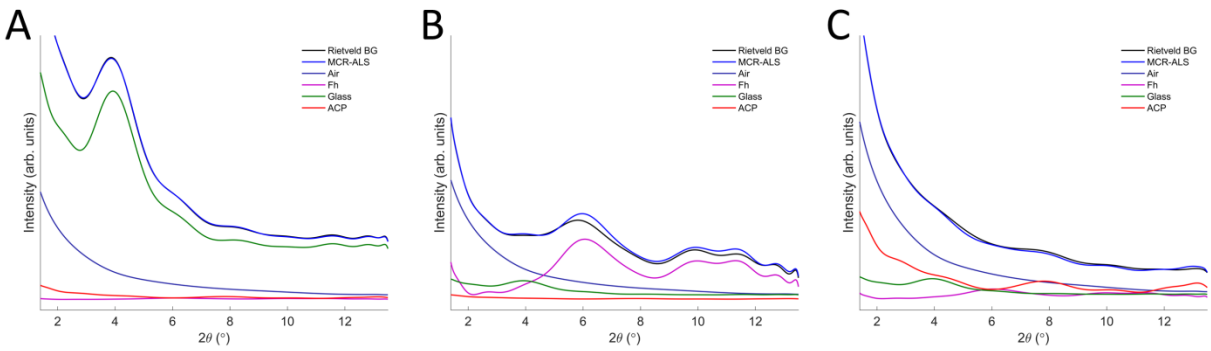

Figure S3 Fitting of the smoothly varying background through MCR-ALS. The data is shown in black and the fit in blue. The four individual components (air, ferrihydrite (Fh), glass and amorphous calcium phosphate (ACP)) are plotted scaled to their concentration in the given point. A) A point primarily containing glass. The fit is perfect and the data and the model are superimposed on one another. B) Data from a voxel primarily containing Fh and air. A small contribution from glass can be detected while the contribution from ACP is zero. C) A point primarily containing Air and ACP with small contributions from glass and Fh.

S5. The importance of distance for reciprocal space resolution

When determining crystalline sizes from peak broadening relatively high resolution in reciprocal space is needed ($\Delta d/d$). Due to the finite size of pixels on detectors, this is in practice limited by the sample to detector distance. This phenomenon is illustrated in figure S2. Here, the uncertainty of the nano crystalline size determined by the Scherrer formula based on the FWHM

of a peak located at θ = 5° is plotted as a function of distance between sample and detector. We assume monodisperse nanocrystals with a size of 10 nm and 50 nm, respectively, and that the peak broadening arises solely from size effects. As in the present experiment, we used an energy of 42.7 keV and a detector pixel size of 200 µm. We calculated the deviation from correct nanocrystal size assuming a 1/2 pixel error (±) in the value of the FWHM. This is seen to severely impact the size determination at low detector to sample distances, especially for large nanocrystal sizes. In our experiments, we used a distance of over 248 cm for which the effect of pixilation of data is below 1 % even for the largest crystals. However, to collect PDF DSCT data with a similar detector (Jacques *et al.*, 2013) requires much smaller sample to detector distances, which in turn results in the large deviations in crystallite size as determined from peak broadening as shown in Figure S2.

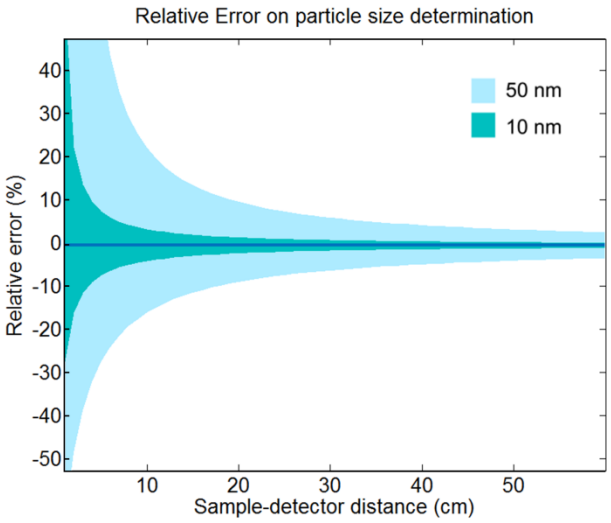

Figure S4 Deviation in nanocrystal size for a crystallite size of 10 and 50 nm assuming 1/2 pixel precision as a function of varying sample to detector distance. The relative error in determining crystal sizes is largest for small sample to detector distances and the effect is largest for large crystallites.

Howard, C. (1982). "The approximation of asymmetric neutron powder diffraction peaks by sums of Gaussians." Journal of Applied Crystallography **15**(6): 615-620.

Jørgensen, J.-E., L. Mosegaard, L. E. Thomsen, T. R. Jensen and J. C. Hanson (2007). "Formation of γ-Fe2O3 nanoparticles and vacancy ordering: An in situ X-ray powder diffraction study." Journal of Solid State Chemistry **180**(1): 180-185.
Meagher, E. P. and G. A. Lager (1979). "Polyhedral thermal expansion in the TiO_2 polymorphs; refinement of the crystal structures of rutile and brookite at high temperature." The Canadian Mineralogist **17**(1): 77-85.
Rezaee, M., S. M. Mousavi Khoie and K. H. Liu (2011). "The role of brookite in mechanical activation of anatase-to-rutile transformation of nanocrystalline TiO2: An XRD and Raman spectroscopy investigation." CrystEngComm **13**(16): 5055-5061.
Thompson, P., D. E. Cox and J. B. Hastings (1987). "Rietveld refinement of Debye-Scherrer synchrotron X-ray data from Al_2O_3." Journal of Applied Crystallography **20**(2): 79-83.
Veselinovic, L., L. Karanovic, Z. Stojanovic, I. Bracko, S. Markovic, N. Ignjatovic and D. Uskokovic (2010). "Crystal structure of cobalt-substituted calcium hydroxyapatite nanopowders prepared by hydrothermal processing." Journal of Applied Crystallography **43**(2): 320-327.